Nonlinear Electron-Phonon Coupling in Doped Manganites

V. Esposito, M. Fechner, R. Mankowsky, H. Lemke, M. Chollet, J. M. Glownia, M. Nakamura, M. Kawasaki, Y. Tokura, U. Staub, P. Beaud, and M. Först

Phys. Rev. Lett. **118**, 247601 — Published 15 June 2017

DOI: 10.1103/PhysRevLett.118.247601

Nonlinear electron-phonon coupling in doped manganites

V. Esposito,[1,*] M. Fechner,[2,3] R. Mankowsky,[2,4] H. Lemke,[5,6] M. Chollet,[5] J.M. Glownia,[5] M. Nakamura,[7] M. Kawasaki,[7,8] Y. Tokura,[7,8] U. Staub,[1] P. Beaud,[1,6] and M. Först[2,4]

[1]*Swiss Light Source, Paul Scherrer Institut, 5232 Villigen PSI, Switzerland*

[2]*Max-Planck Institute for the Structure and Dynamics of Matter, 22761 Hamburg, Germany*

[3]*Materials Theory, ETH Zürich, Wolfgang-Pauli-Strasse 27, 8093 Zürich, Switzerland*

[4]*Center for Free Electron Laser Science, 22761 Hamburg, Germany*

[5]*LCLS, SLAC National Accelerator Laboratory, Menlo Park, California 94025, USA*

[6]*SwissFEL, Paul Scherrer Institut, 5232 Villigen PSI, Switzerland*

[7]*RIKEN Center for Emergent Matter Science, Wako 351-0198, Japan*

[8]*Department of Applied Physics and Quantum Phase Electronics Center (QPEC), University of Tokyo, Tokyo 113-8656, Japan*

(Dated: April 26, 2017)

Abstract

We employ time-resolved resonant x-ray diffraction to study the melting of charge order and the associated insulator-to-metal transition in the doped manganite $Pr_{0.5}Ca_{0.5}MnO_3$ after resonant excitation of a high-frequency infrared-active lattice mode. We find that the charge order reduces promptly and highly nonlinearly as function of excitation fluence. Density functional theory calculations suggest that direct anharmonic coupling between the excited lattice mode and the electronic structure drives these dynamics, highlighting a new avenue of nonlinear phonon control.

Some of the most fascinating phenomena in condensed matter physics arise from electron-phonon interactions. A striking example is the BCS theory for superconductivity, where phonons mediate an attractive interaction between two electrons with opposite spin and momentum to allow the carriers to condensate into the superconducting state [1]. In metals and semiconductors, transport properties are also shaped by linear electron-phonon (e-ph) coupling, in particular through the creation of polarons [2]. Furthermore, e-ph coupling plays an important role in the physics of perovskite oxides such as the mixed-valence manganites, where a variety of electronic and magnetic phases is stabilized via the Jahn-Teller effect [3]. The precarious equilibrium between these possible ground states is easily perturbed by external stimuli such as static electric or magnetic fields, temperature, pressure or even by light, opening new ways of manipulating matter on ever faster timescales with short laser pulses [4–10].

The recent progress in the generation of high-energy ultrashort pulses in the mid-infrared (mid-IR) range permits to resonantly excite vibrational modes of the lattice to large amplitudes, exceeding several percent of the interatomic distances — a value at which nonlinear coupling of phonons to other degrees of freedom becomes important [11–13]. This approach enabled mode-selective material control on sub-picosecond timescales, as exemplified in the possible enhancement of superconductivity [8, 12], the occurrence of insulator-metal transitions and the suppression of magnetic and orbital order in manganites [11, 14]. A proposed mechanism, referred to as 'nonlinear phononics' and based on nonlinear phonon-phonon coupling, suggests that these phenomena result from the rectification of the excited mode and a net displacement of the crystal lattice along the coordinates of anharmonically coupled vibrational modes, which control the electronic properties [8, 14–16]. However, a possible direct coupling between the excited mode and the electronic system has only seldomly been considered [17], although, for example, the vibrational excitation of a molecular solid was shown to coherently perturb the electronic interactions by directly affecting the orbital wave functions [18].

In this Letter, we explore the nonlinear electron-phonon coupling in a manganite by investigating the lattice driven ultrafast insulator-metal transition. We use resonant x-ray diffraction at the Mn K edge to study the dynamics of the electronic and structural order in a $Pr_{0.5}Ca_{0.5}MnO_3$ (PCMO) thin film driven by large-amplitude excitation of a vibrational mode with 200 fs mid-IR pulses, which was previously shown to induce a metallic state [11].

We then compare our experimental findings with *ab initio* calculations.

At room temperature, $Pr_{0.5}Ca_{0.5}MnO_3$ is a paramagnetic semiconductor that undergoes a large distortion of the cubic perovskite structure. Charge and orbital order (COO) and antiferromagnetic (AFM) phases arise upon cooling below T_{CO} = 240 K and T_N = 150 K respectively [3]. This so-called CE-type COO is characterized by a zig-zag arrangement of the *3d* e_g orbitals and a checkerboard pattern of Mn^{3+}/Mn^{4+}ions (Fig. 1 (a)). The long range ordering of the electrons goes in hand with a structural distortion due to the Jahn-Teller effect at the Mn^{3+} sites that lowers the crystal symmetry from orthorhombic *Pbnm* to monoclinic $P2_1/m$ and a doubling of the unit cell along the *b* axis, leading to weak superlattice reflections of the type $(h\frac{k}{2}l)$.

The 40 nm PCMO thin film was grown by pulsed laser deposition on a (011)-oriented LSAT substrate, as described in [20] and has an ordering temperature T_{CO} of 220 K, only slightly below the reported bulk critical temperature. During the experiment, the sample was kept at 100 K, well below T_{CO} by means of a nitrogen cryo-blower. The sample was excited with 200 fs mid-IR pulses produced by mixing the signal and idler from a high energy optical parametric amplifier (OPA) seeded by the 800nm output of an amplified Ti:S laser. The OPA output wavelength was tuned to the stretching mode of the apical Mn-O bond ($\lambda \approx 17$ μm, bandwidth 1.5 μm) with a maximum energy per pulse of 33 μJ (Fig. 1 (b)). The subsequent dynamics were probed by resonant X-ray diffraction at the Mn K edge with monochromatized 50 fs pulses provided by the LCLS free electron laser at the SLAC National Accelerator Laboratory. To guarantee an optimum time resolution the arrival time difference between the pump and the probe was measured shot-to-shot by means of the spectral encoding technique [21]. A sketch of the pump-probe experiment that was carried out at the XPP instrument [22] is shown in Fig. 1 (c). The probed area is homogenously excited due to the relatively large 280 x 750 μm^2 pump spot (versus 50 x 50 μm^2 for the X-ray beam). P-polarized light ensures maximum power transmitted into the sample. Because the penetration depth of the mid-IR (360 nm) is much larger than the film thickness (40 nm), the excitation density can be considered as uniform over the entire probed volume. Optimization of various geometrical constraints leads to the non-collinear geometry of the experiment (see Fig. 1 (c)), more details can be found in the Supplementary Informations [23].

The charge order response is measured by the intensity of the $(0\bar{3}0)$ reflection at the Mn

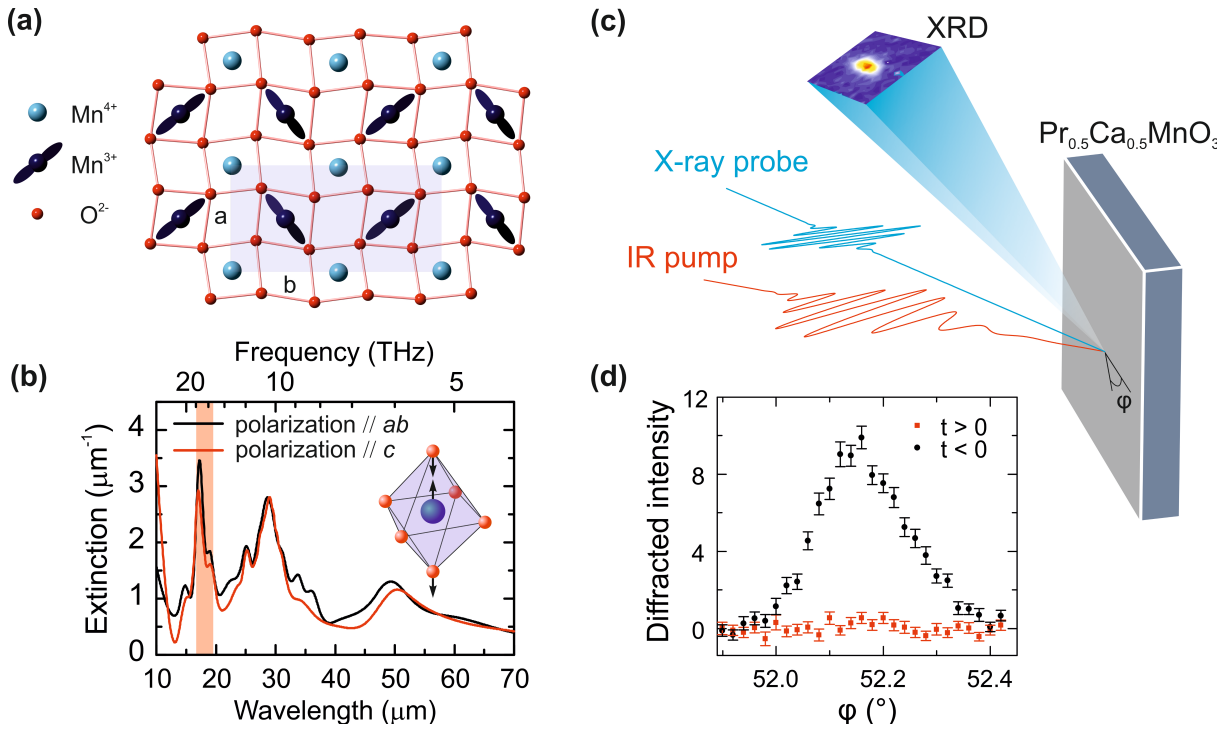

FIG. 1. (a) Charge and orbital order in PCMO in the *ab*-plane. The low temperature unit cell is delimited by the blue shaded area. (b) Absorption spectra of a $Nd_{0.5}Ca_{0.5}MnO_3$ single crystal in the mid-IR range (reproduced from ref. [19]). This materials displays a very similar phase diagram than PCMO and has the same structure and COO pattern below T_{CO}. The shaded red area represents spectral range of the pump. The inset shows the dominant motion driven by the excitation. (c) Experimental setup at the XPP beamline at the LCLS. The angle ϕ indicates the rotation angle around the sample's surface normal. (d) Rotational scan around the sample surface normal (angle in panel c) of the $(0\bar{3}0)$ reflection before and 4 ps after excitation at a pump fluence of 10.7 mJ/cm^2. The complete suppression of the Bragg peak after photo-excitation demonstrates the melting of the COO.

K edge, which directly relates to the charge disproportionation at the Mn sites [24]. Figure 1 (d) shows the disappearance of the $(0\bar{3}0)$ Bragg peak 200 femtoseconds after excitation at a fluence of 10.7 mJ/cm^2, demonstrating complete charge and orbital order melting. The dynamics of the charge order peak for different excitation fluence are shown in Figure 2 (a). Minor intensity changes are observed below 5 mJ/cm^2. Above a critical fluence of $f_c = 8.7$ mJ/cm^2, the $(0\bar{3}0)$ reflection disappears within the experimental time resolution of 200 fs, clearly evidencing prompt CO melting. In a narrow range of intermediate fluences,

the CO is only partially melted and recovers over several tens of picoseconds. The fluence dependence of the intensity drop, shown in Figure 2 (b), highlights this nonlinear, threshold-like behavior. In contrast, above-bandgap-excitation at near-IR 800 nm wavelengths, which directly perturbs the electronic system, results in prompt charge order melting with a linear fluence dependence [10], as shown in the overlaid data.

We performed DFT calculations to identify the lattice dynamics induced by the intense mid-infrared excitation and their effects on the electronic structure. The first principle calculations are performed in the framework of density functional theory using the generalized gradient approximation (GGA) [25] as implemented within the Vienna ab-initio simulation package (VASP) [26]. All our calculations are done with the default projector augmented wave (PAW) pseudopotentials [27] which exhibit the following electronic configurations: Pr ($6p^1$, $6s^2$, $5p^6$,$5s^2$), Ca ($3s^2$,$3p^6$), Mn ($3d^5$, $4s^2$, $3p^6$) and O ($2s^2$, $2p^4$). To take into account strong correlation effects, we employ a *DFT+U* scheme [28] with $U = 5.0$ eV and $J = 0.0$ eV applied to the Mn d-states. We select these values to reproduce the experimental band gap of 0.37 eV [29]. After testing the convergence of forces, phonon frequencies and anharmonic coupling constants, we chose a 3x5x7 k-point mesh in combination with a cutoff energy for the plane wave basis set of 550 eV. We further perform structural relaxations, to obtain force free reference structures, required for computations of the phonon spectra. The convergence thresholds for the electronic and ionic steps are set to 10^{-8} eV and 0.1 meV/Å respectively. More details on the phonon calculations are given in the Supplementary Informations [23]. The analysis of the zone-center phonon modes reveals that only two infrared-active (IR) modes at 17.2 and 18.9 THz are significantly excited by the c-axis polarized mid-IR pulse. The ionic motion of these modes, which besides the main Mn-O stretching sketched in Fig. 1 (b) also exhibit small displacements within the ab-plane, are presented in the Supplementary Information [23]. First, we consider the anharmonic coupling of these modes to Raman modes within the framework of nonlinear phononics. As opposed to Ref. 17, however, we use the low temperature charge ordered $P2_1/m$ structure [23]. Mapping the total energies of our DFT calculations onto the full phonon-phonon potential $V = \omega_{IR}^2 Q_{IR}^2 + \omega_R^2 Q_R^2 + a_3 Q_R Q_{IR}^2 + ...$, we find that both excited IR modes couple only weakly (as a_3/ω_R^2) to Raman modes, displacing the lattice along the coordinates of low frequency Ag modes by maximum 0.05 $\sqrt{u}$Å [23]. This atomic motion is by more than one order of magnitudes smaller than observed in $YBa_2Cu_3O_{6.5}$, where the enhancement of

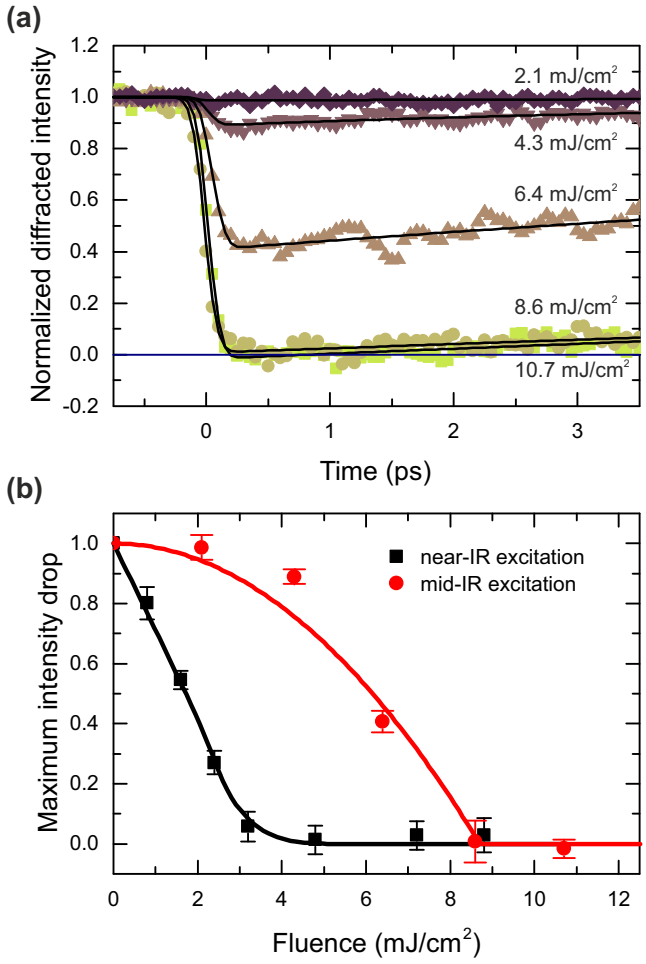

FIG. 2. Dynamic of charge order melting. (a) Transient response of the $(0\bar{3}0)$ charge order reflection for different fluence ($\lambda = 17$ μm). The time traces were taken at the maximum intensity of the Bragg peak (Fig. 1 (d)). The error bars are about 1.5 times the symbol size and are not displayed for clarity. The black lines are fits to the data consisting of an error function with an exponential recovery. (b) Whereas excitation with near-IR pulses leads to a linear drop in diffraction intensity as a function of fluence and can be described by the Landau-type order parameter proposed in Ref. [10] (black squares and line), the intensity drop following mid-IR excitation is highly non-linear. The red circles are the maximal drop given from the fit of the time evolution traces and the red line is a fit using $1 - \left(\frac{f}{f_c}\right)^2$ yielding a critical fluence of 8.7 ± 0.7 mJ/cm^2.

superconductivity was shown to be the consequence of such lattice anharmonicity [8, 16]. Furthermore, the PCMO bandgap reduction induced by the atomic motions of the non-linearly coupled A_g Raman modes scales linearly with the excitation fluence [23], overall suggesting that the nonlinear phononics mechanism is likely not driving the insulator-metal transition.

Hence, we explore the changes of the electronic structure due to the atomic displacement along the coordinates of the directly excited IR mode. The CO state is stabilized by the creation of an electronic gap (E_g), whose lattice-induced alterations are computed within the frozen phonon approximation for both modes. We find a quartic reduction of the gap size as a function of both mode amplitudes, which at large values close the band gap as shown in Fig. 3 (a).

To confront this finding with the experimental observation, we calculate the fluence dependent amplitudes of the IR modes by numerically solving the equations of motion [30]. For simplicity, we assume that the electronic gap is determined by the maximum phonon amplitude $Q^4_{\mathrm{IR,max}}$ of the directly driven phonon modes, which is reached at the end of the mid-IR excitation pulse. However, we cannot rule out that dynamically the gap size reduces with the time-average $\langle Q^4_{\mathrm{IR}} \rangle$ of these modes. Figure 3 (b) shows the calculated gap size for both individually excited modes and their summed contribution, revealing a critical pump fluence of $f_c = 5.4$ mJ/cm^2 for a full gap closure. This value is slightly lower than the experimental value of 8.7 mJ/cm^2. However, when taking into account the 32° angle between the mid-IR pump electric field and the c-axis, the estimated experimental critical fluence reduces by 28% to $f_c \approx 6.3$ mJ/cm^2, which is in excellent agreement with the calculation. As both the calculated gap energy and the measured (03 0) Bragg intensity represent the square of the charge order parameter [31], these quantities can be directly compared. A quadratic function fit, as expected from the square reduction of the gap energy with excitation fluence, reproduces the measured diffracted intensity drop reasonably well (see Fig. 2 (b)).

We further probed the dynamics of the crystal lattice by measuring two superlattice reflections (Fig. 4): the $(0\frac{\bar{5}}{2}0)$ peak, sensitive to the Jahn-Teller distortion and orbital order at the Mn^{3+} sites, and the $(\bar{2}\frac{\bar{3}}{2}0)$, a direct measure of the overall structural distortion that accompanies the charge and orbital ordering. The fast drop in diffracted intensity and the coherent 2.4 THz modulations for both reflections indicate a displacive excitation of atomic motions towards the high-symmetry phase triggered by the melting of the CO/OO [10, 32].

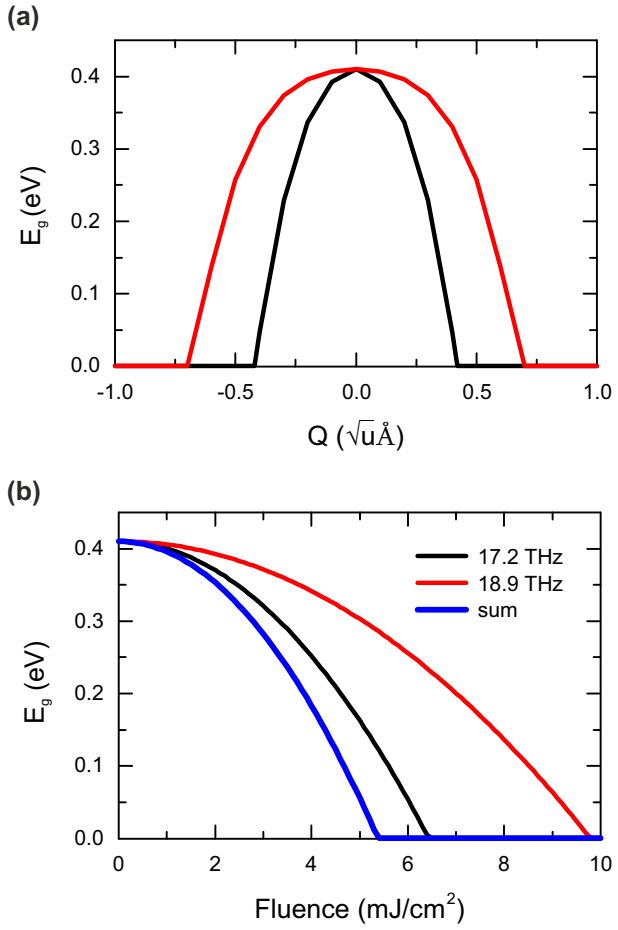

FIG. 3. (a) Calculated gap energy as a function of the frozen amplitude of the two excited IR modes. Interestingly, the quadratic coefficient also vanishes and the coupling is found to be purely quartic. The phonon amplitude Q is given in units of $\sqrt{u}$Å, where u is the atomic mass. (b) The electronic gap as a function of mid-IR fluence for the two excited IR modes and their summed contribution. All other contributions, from additional IR modes or coupled Raman phonon are found to be negligible (see Suppl. Materials).

The same relaxation and coherent dynamics were observed earlier when prompt melting of the charge order was induced by direct excitation of the electronic system [10]. These similarities suggest that the structural dynamics are initiated by CO melting in both cases.

The phenomenological model, describing charge order dynamics induced by exciting the electronic system in the near-IR, proposes the charge order parameter $\eta = \sqrt{1 - \frac{n}{n_c}}$ in the driven state to depend solely on the excess energy in the electronic system [10]. A critical

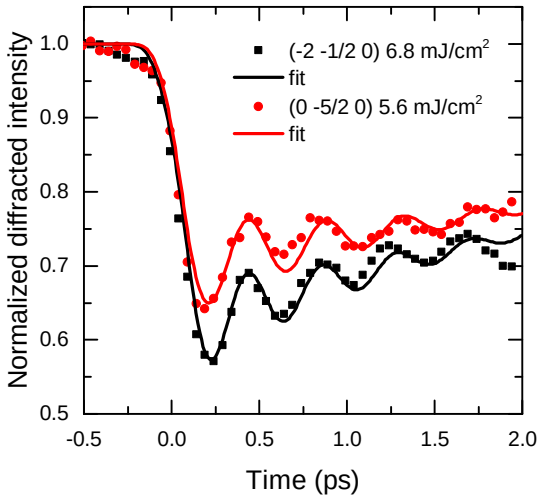

FIG. 4. Response of the structural superlattice reflection $(\bar{2}\frac{\bar{3}}{2}0)$ and the orbital order reflection $(0\frac{\bar{5}}{2}0)$ at intermediate pump fluence. As for excitation of the electronic system at near-IR wavelength, a 2.4 THz coherent oscillation around a new equilibrium position is observed, suggesting a displacive excitation mechanism triggered by the fast melting of charge and orbital order in both cases. The solid lines are fits of an exponential recovery and a damped oscillation.

excitation density of 500 J/cm^3 was required for the phase transition to occur. Assuming linear extinction, direct lattice excitation investigated here requires a significantly lower critical excitation density of 200 J/cm^3.

Once the electronic gap becomes smaller than the mid-infrared photon energy, direct photo-doping into the electronic system sets in, possibly leading to nonlinear absorption. The details of these dynamics could be experimentally investigated by monitoring the CO during the pump pulse, an experiment that requires carrier-envelope phase-stable mid-IR pulses and a high time resolution. Further insight on the energy balance between the lattice and the electrons will be gained once time-resolved dynamical calculations will become feasible for such large systems. In addition, a comprehensive characterization of the photo-induced transient state is still missing and other crucial aspects of the transition need to be explored. The spin dynamics and the magnetic ordering have been completely ignored here [33], yet in the manganites transport properties are tightly bound to the magnetic state.

In summary, we have shown that the melting of the charge and orbital order following coherent lattice excitation in PCMO are driven by the direct and highly nonlinear coupling

between the excited IR modes and the electronic degrees of freedom. As the gap closes, the charge and orbital order is suppressed and the Jahn-Teller distortion released, triggering structural relaxation. When combined with DFT calculations, the observed nonlinear behavior is well explained by the quartic dependence of the electronic gap on the excited phonon coordinate. This is an example of a new and direct way of phonon control of materials, where the electron-phonon interaction is pushed to the nonlinear regime, allowing the coupling with odd-parity modes.

This work was supported by the NCCR Molecular Ultrafast Science and Technology (NCCR MUST), research instrument of the Swiss National Science Foundation (SNSF). Use of the Linac Coherent Light Source (LCLS), SLAC National Accelerator Laboratory, is supported by the U.S. Department of Energy, Office of Science, Office of Basic Energy Sciences under Contract No. DE-AC02-76SF00515. M.N. was supported by the Japan Science and Technology Agency (JST), PRESTO.

* Corresponding author: vincent.esposito@psi.ch

[1] J. Bardeen, L. N. Cooper, and J. R. Schrieffer, Phys. Rev. **108**, 1175 (1957).

[2] G. D. Mahan, *Many-particle physics*, 3rd ed. (Springer Science & Business Media, 2000).

[3] E. Dagotto, *Nanoscale phase separation and colossal magnetoresistance: the physics of manganites and related compounds* (Springer, 2003).

[4] K. Miyano, T. Tanaka, Y. Tomioka, and Y. Tokura, Phys. Rev. Lett. **78**, 4257 (1997).

[5] F. Schmitt, P. S. Kirchmann, U. Bovensiepen, R. G. Moore, L. Rettig, M. Krenz, J.-H. Chu, N. Ru, L. Perfetti, D. Lu, *et al.*, Science **321**, 1649 (2008).

[6] T. Kampfrath, A. Sell, G. Klatt, A. Pashkin, S. Mährlein, T. Dekorsy, M. Wolf, M. Fiebig, A. Leitenstorfer, and R. Huber, Nature Photonics **5**, 31 (2011).

[7] G. Coslovich, B. Huber, W.-S. Lee, Y.-D. Chuang, Y. Zhu, T. Sasagawa, Z. Hussain, H. Bechtel, M. Martin, Z.-X. Shen, *et al.*, Nat. Comm. **4** (2013).

[8] R. Mankowsky, A. Subedi, M. Först, S. Mariager, M. Chollet, H. Lemke, J. Robinson, J. Glownia, M. Minitti, A. Frano, *et al.*, Nature (London) **516**, 71 (2014).

[9] T. Kubacka, J. A. Johnson, M. C. Hoffmann, C. Vicario, S. de Jong, P. Beaud, S. Grübel, S.-W. Huang, L. Huber, L. Patthey, Y.-D. Chuang, J. J. Turner, G. L. Dakovski, W.-S. Lee, M. P.

Minitti, W. Schlotter, R. G. Moore, C. P. Hauri, S. M. Koohpayeh, V. Scagnoli, G. Ingold, S. L. Johnson, and U. Staub, Science **343**, 1333 (2014).

[10] P. Beaud, A. Caviezel, S. Mariager, L. Rettig, G. Ingold, C. Dornes, S. Huang, J. Johnson, M. Radovic, T. Huber, *et al.*, Nat. Mater. **13**, 923 (2014).

[11] M. Rini, N. Dean, J. Itatani, Y. Tomioka, Y. Tokura, R. W. Schoenlein, A. Cavalleri, *et al.*, Nature (London) **449**, 72 (2007).

[12] D. Fausti, R. Tobey, N. Dean, S. Kaiser, A. Dienst, M. C. Hoffmann, S. Pyon, T. Takayama, H. Takagi, and A. Cavalleri, Science **331**, 189 (2011).

[13] M. Först, C. Manzoni, S. Kaiser, Y. Tomioka, Y. Tokura, R. Merlin, and A. Cavalleri, Nat. Phys. **7**, 854 (2011).

[14] M. Först, R. I. Tobey, S. Wall, H. Bromberger, V. Khanna, A. L. Cavalieri, Y.-D. Chuang, W. S. Lee, R. Moore, W. F. Schlotter, J. J. Turner, O. Krupin, M. Trigo, H. Zheng, J. F. Mitchell, S. S. Dhesi, J. P. Hill, and A. Cavalleri, Phys. Rev. B **84**, 241104 (2011).

[15] A. Subedi, A. Cavalleri, and A. Georges, Phys. Rev. B **89**, 220301 (2014).

[16] M. Fechner and N. A. Spaldin, Phys. Rev. B **94**, 134307 (2016).

[17] M. Kim, Y. Nomura, M. Ferrero, P. Seth, O. Parcollet, and A. Georges, Phys. Rev. B **94**, 155152 (2016).

[18] R. Singla, G. Cotugno, S. Kaiser, M. Först, M. Mitrano, H. Y. Liu, A. Cartella, C. Manzoni, H. Okamoto, T. Hasegawa, S. R. Clark, D. Jaksch, and A. Cavalleri, Phys. Rev. Lett. **115**, 187401 (2015).

[19] K. Tobe, T. Kimura, and Y. Tokura, Phys. Rev. B **69**, 014407 (2004).

[20] D. Okuyama, M. Nakamura, Y. Wakabayashi, H. Itoh, R. Kumai, H. Yamada, Y. Taguchi, T. Arima, M. Kawasaki, and Y. Tokura, Appl. Phys. Lett. **95**, 152502 (2009).

[21] M. Harmand, R. Coffee, M. Bionta, M. Chollet, D. French, D. Zhu, D. Fritz, H. Lemke, N. Medvedev, B. Ziaja, *et al.*, Nat. Phot. **7**, 215 (2013).

[22] M. Chollet, R. Alonso-Mori, M. Cammarata, D. Damiani, J. Defever, J. T. Delor, Y. Feng, J. M. Glownia, J. B. Langton, S. Nelson, K. Ramsey, A. Robert, M. Sikorski, S. Song, D. Stefanescu, V. Srinivasan, D. Zhu, H. T. Lemke, and D. M. Fritz, Journal of Synchrotron Radiation **22**, 503 (2015).

[23] See Supplemental Material [url] for additional informations on the experimental geometry and the *ab initio* phonon calculation, which includes Refs. [34, 35].

[24] M. v. Zimmermann, J. P. Hill, D. Gibbs, M. Blume, D. Casa, B. Keimer, Y. Murakami, Y. Tomioka, and Y. Tokura, Phys. Rev. Lett. **83**, 4872 (1999).

[25] J. P. Perdew, K. Burke, and M. Ernzerhof, Physical review letters **77**, 3865 (1996).

[26] G. Kresse and J. Furthmüller, Physical review B **54**, 11169 (1996).

[27] P. E. Blöchl, Physical Review B **50**, 17953 (1994).

[28] V. I. Anisimov, F. Aryasetiawan, and A. Lichtenstein, Journal of Physics: Condensed Matter **9**, 767 (1997).

[29] Y. Okimoto, Y. Tomioka, Y. Onose, Y. Otsuka, and Y. Tokura, Phys. Rev. B **59**, 7401 (1999).

[30] D. M. Juraschek, M. Fechner, and N. A. Spaldin, arXiv preprint arXiv:1607.01653 (2016).

[31] K. A. Ross, Y. Qiu, J. R. D. Copley, H. A. Dabkowska, and B. D. Gaulin, Phys. Rev. Lett. **112**, 057201 (2014).

[32] A. Caviezel, S. O. Mariager, S. L. Johnson, E. Möhr-Vorobeva, S. W. Huang, G. Ingold, U. Staub, C. J. Milne, S.-W. Cheong, and P. Beaud, Phys. Rev. B **87**, 205104 (2013).

[33] T. Li, A. Patz, L. Mouchliadis, J. Yan, T. A. Lograsso, I. E. Perakis, and J. Wang, Nature **496**, 69 (2013).

[34] R. J. Goff and J. P. Attfield, Phys. Rev. B **70**, 140404 (2004).

[35] A. Togo and I. Tanaka, Scripta Materialia **108**, 1 (2015).